Materials Chemistry and Physics 246 (2020) 122812

Contents lists available at ScienceDirect

Materials Chemistry and Physics

journal homepage: www.elsevier.com/locate/matchemphys

Magnetic-field-induced synthesis of amorphous iron-nickel wire-like nanostructures

Marcin Krajewski [a,*], Mateusz Tokarczyk [b], Tomasz Stefaniuk [b], Hanna Słomińska [a], Artur Małolepszy [c], Grzegorz Kowalski [b], Sabina Lewińska [d], Anna Ślawska-Waniewska [d]

[a] Institute of Fundamental Technological Research, Polish Academy of Sciences, Pawińskiego 5B, 02-106, Warsaw, Poland
[b] Faculty of Physics, Institute of Experimental Physics, University of Warsaw, Pasteura 5, 02-093, Warsaw, Poland
[c] Faculty of Chemical and Process Engineering, Warsaw University of Technology, Waryńskiego 1, 00-645, Warsaw, Poland
[d] Institute of Physics, Polish Academy of Sciences, Al. Lotników 32/46, 02-668, Warsaw, Poland

HIGHLIGHTS

- Formation of amorphous wire-like nanomaterials via magnetic-field-induced synthesis.
- Synthesis procedures of Fe–Ni wire-like nanostructures are provided.
- Fe–Ni wire-like materials consist of nanoparticles and reveal core-shell structures.
- Investigated wire-like nanochains are ferromagnetic nanoalloys.

ARTICLE INFO

Keywords:
Amorphous materials
Fe–Ni chains
Magnetic-field-induced synthesis
Magnetic materials
Wire-like nanostructure

ABSTRACT

Manufacturing process of wire-like binary or ternary metal nanoalloys applying the magnetic-field-induced (MFI) synthesis is still a challenging task. Hence, this work demonstrates for the first time how to produce the iron-nickel wire-like nanostructures with $Fe_{0.75}Ni_{0.25}$, $Fe_{0.5}Ni_{0.5}$ and $Fe_{0.25}Ni_{0.75}$ compositions. In a contrary to the previously reported synthesis of the Fe–Ni wire-like nanomaterials, this process has been carried out at room temperature without employment of templates, surfactants, organic solvents, and other chemical additives. The as-prepared samples exhibit specific structures with the amorphous bimetallic alloy cores covered by thin amorphous oxide shells. Moreover, they are composed of nanoparticles which are aligned in nearly linear chains. The Fe–Ni samples are ferromagnetic materials. Their coercivity values and saturation magnetizations depend on chemical compositions and dimensions of the investigated chains. The highest saturation magnetization and the lowest coercivity is found for the material with the lowest content of nickel and vice versa.

1. Introduction

One-dimensional (1D) nanostructures such as chains, rods, tubes, fibers, and wires are one of the most frequently studied nanomaterials [1,2]. This is associated with the fact that they offer unique chemical, physical as well as mechanical properties in a comparison with their bulk counterparts [3]. Besides that, their properties can be easily-controlled by changing their length to diameter ratios i.e. aspect ratios [4]. All these features cause that 1D nanomaterials are often considered as an important building block of numerous applications, such as: energy storage and conversion devices, catalysts, sensors, etc. [5–7].

Various synthesis procedures leading to the wire-like nanostructures formation have been proposed so far [2–4]. Among them, the relatively new concept gains more and more attention in the scientific community which is associated with the usage of an external magnetic field as a synthesis parameter. This approach is commonly called as the magnetic-field-assisted (MFA) or magnetic-field-induced (MFI) synthesis and allows manufacturing a large amount of long wire-like nano-objects during a single run of synthesis. Nevertheless, due to the unpredictable growth of either binary or ternary wire-like metal nanostructures, one of unexplored areas related to the MFI synthesis remains their cheap and high-yield production [2]. As far as we know, only few publications have appeared which demonstrate the application of MFI

* Corresponding author.
E-mail address: mkraj@ippt.pan.pl (M. Krajewski).

https://doi.org/10.1016/j.matchemphys.2020.122812
Received 17 July 2019; Received in revised form 10 February 2020; Accepted 13 February 2020
Available online 15 February 2020

thermal decomposition [8] as well as MFI solvothermal and chemical reduction as processes leading to obtain binary metal nanowires [9–13]. This indicates clearly that the use of MFI synthesis to produce binary metal wire-like nanomaterials constitutes still a challenging task.

Among the binary metal nanostructures, the ferromagnetic iron nickel (Fe–Ni) alloy is very interesting due to its practical application in catalysis, electromagnetic shielding, microwave-absorbents and magnetic field sensors [14–17]. It is also known that by changing the iron-to-nickel composition in alloy it is possible to adjust its properties [17–20]. Nevertheless, no research report, which describes the possible MFI synthesis of the Fe_xNi_{1-x} nanoalloy (x = 0.25 or 0.50 or 0.75) in details, has been published so far. Therefore, this work aims to develop the current knowledge in this field and demonstrates for the first time the novel procedures leading to the formation of the Fe–Ni wire-like nanostructures containing various iron-to-nickel ratios.

2. Experimental

2.1. Fabrication of iron-nickel wire-like nanostructures

Iron-nickel wire-like nanostructures were manufactured by combining two well-known processes, namely, i) the magnetic-field-induced chemical reduction which allows producing iron nanowires [21,22], and ii) the chemical reduction of iron and nickel ions with sodium borohydride [19]. In order to produce the nanomaterials with the $Fe_{0.75}Ni_{0.25}$, $Fe_{0.5}Ni_{0.5}$ and $Fe_{0.25}Ni_{0.75}$ compositions, three precursor solutions were prepared by dissolution of 1.315 g, 0.865 g, 0.427 g of iron(II) chloride hydrate ($FeCl_2{\cdot}xH_2O$; 98%, Carl Roth GmbH) and 0.524 g, 1.035 g, 1.532 g of nickel(II) chloride hexahydrate ($NiCl_2{\cdot}6H_2O$; 97%, Carl Roth GmbH), respectively, in 300 ml of deionized water. Then, each mixture was placed in a separate glass reactor covered with a three-neck cap. One side neck was used as an inlet of inert gas (argon; >99%, BialGaz Company), whereas the second one constituted a gas outlet. The middle neck was connected with a dropping funnel where 1.4 g of sodium borohydride ($NaBH_4$; 97%, Carl Roth GmbH) dissolved in 175 ml of deionized water was placed. The inert gas was bubbling through the solution during the whole reaction as well as for about 5 min after adding the last drop of $NaBH_4$. This allowed purging out the dissolved oxygen as well as provided stirring of the precursor solutions. Moreover, the reaction was performed in the average external magnetic field of about 0.05 T which was generated by two parallel neodymium magnets. The addition of reducing agent into the precursor solution caused the discoloration of initial solution and at the same time the formation of black precipitations floating perpendicularly to the reactor walls. These black powders were formed according to the following chemical equation:

$$x\ FeCl_2 + (1-x)\ NiCl_2 + 2\ NaBH_4 + 6\ H_2O \rightarrow Fe_xNi_{1-x}\downarrow + 2\ H_3BO_3 + 2\ NaCl + 7\ H_2\uparrow \quad (1)$$

where x is 0.75, 0.5 or 0.25.

The obtained materials were washed three times with ethanol (99.8%, Avantor (POCH)) and three times with acetone (99.5%, Carl Roth GmbH) in order to remove the reaction by-products. Afterwards, they were dried in a vacuum oven at 50 °C for 2 h.

2.2. Characterization of wire-like nanostructures

The morphology of investigated nanostructures was determined with a Zeiss Sigma scanning electron microscope (SEM) and a JEOL – JEM 1011 transmission electron microscope (TEM). The chemical composition was examined using a Bruker XFlash 6|10 energy dispersive X-ray spectrometer (EDS), a JOEL EDS JSM-6010LA (EDS), and a Malvern Panalytical Epsilon 3XLE energy dispersive X-ray fluorescence (EDXRF) spectrometer. The X-ray diffraction (XRD) measurements were carried out on a Phillips X'Pert Diffractometer equipped with a Cu X-ray lamp and a parallel beam Bragg reflection mirror. The magnetic properties were determined at room temperature by means of an Oxford Instruments Ltd. vibrating sample magnetometer (VSM). At this point, it should be noted that the orientations of the investigated chains were random in respect to the external magnetic field during the magnetic measurements.

3. Results and discussion

The morphologies of as-prepared iron-nickel nanomaterials are determined based on the results shown in Fig. 1. In a contrary to the previously reported synthesis of the Fe–Ni nanoparticles [19], the application of the external magnetic field during the manufacturing process causes the formation of nanostructures which exhibit a specific construction. Namely, they are characterized by a segmented structure in which each section is built of a single nanoparticle. Furthermore, these nanoparticles are aligned in long chains which are almost straight. Therefore, the obtained samples can be referred as wire-like nanostructures. According to the presented SEM images, the diameters of nanoparticles forming all as-prepared samples range between 20 and 130 nm, whereas their average values are 68 nm, 71 nm and 49 nm for $Fe_{0.75}Ni_{0.25}$, $Fe_{0.5}Ni_{0.5}$ and $Fe_{0.25}Ni_{0.75}$ chains, respectively. In fact, these mean sizes of diameters are much larger than that for the Fe–Ni nanoparticles obtained in the synthesis without the external magnetic field by A.P. Douvalis et al. [19]. The longest chains are found for the $Fe_{0.25}Ni_{0.75}$ sample. They can exceed over 3 μm but their average length is about 2 μm. In turn, the lengths of $Fe_{0.75}Ni_{0.25}$ and $Fe_{0.5}Ni_{0.5}$ wire-like nanomaterials are more uniformly distributed in a comparison with the $Fe_{0.25}Ni_{0.75}$ chains and they oscillate around 1 μm. In general, at this moment it is hardly difficult to explain why one Fe–Ni nanoparticles forming wire-like structures are much smaller than others. Undoubtedly, this is associated with the growth mechanism which is still not clear for binary or ternary metal nanoalloys. Nevertheless, our results are in a good agreement with the observations of M.J. Hu et al. [9] and M.Z. Wu et al. [10] who have noticed that the diameters and lengths vary for the wire-like Ni–Co materials with different nickel-to-cobalt ratios prepared through the MFI solvothermal method. It is also worth noting that the amount of reactants taken to all performed MFI syntheses is the same. Assuming that they have been entirely consumed during the reaction, it is expected that the longest chains should possess the shortest diameters and vice-versa. This, in fact, is valid for the Fe–Ni wire-like nanostructures obtained in this work.

The chemical compositions of the Fe–Ni chains are determined using the EDS and EDXRF techniques and their results are collected in Table 1. Analyzing the obtained data, one can see that both methods are complementary. They indicate that all of Fe–Ni wire-like nanomaterials are mainly composed of Fe and Ni atoms and their distributions correspond well to the composition of initial concentrations of particular ions taken to the reaction. It is also evident that all of investigated samples contain a certain amount of oxygen. Undoubtedly, this is associated with the formation of thin oxide layer on the surface like in many nanomaterials containing significant amount of iron, nickel and/or cobalt [10,19,22,23].

The EDS spectra have been collected from five to six randomly chosen points located in the middle of different chains and then the average content of iron, nickel and oxygen has been estimated for these measurements. In turn, the EDXRF experiments have been performed on few milligrams of each sample. The obtained results from both techniques inform about the average mass percentage of Fe, Ni and other elements in the investigated Fe–Ni nanochains. Since these measurements cannot provide information whether a single wire-like chain is composed of iron and nickel in form of alloy-type or core-shell structure, two other experiments, namely, the line EDS profiles along and across wire-like chain as well as the TEM measurements have been performed for a single $Fe_{0.75}Ni_{0.25}$, $Fe_{0.5}Ni_{0.5}$ and $Fe_{0.25}Ni_{0.75}$ chains.

The SEM images and the corresponding line EDS profiles along and

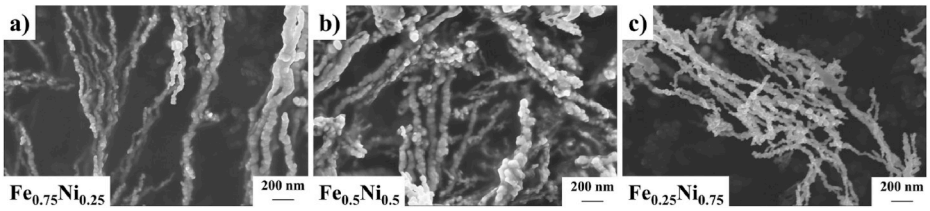

Fig. 1. SEM images of **(a)** $Fe_{0.75}Ni_{0.25}$, **(b)** $Fe_{0.5}Ni_{0.5}$ and **(c)** $Fe_{0.25}Ni_{0.75}$ wire-like nanostructures (magnification 100 000 times).

Table 1
Mass share of iron, nickel and oxygen in the $Fe_{0.75}Ni_{0.25}$, $Fe_{0.5}Ni_{0.5}$ and $Fe_{0.25}Ni_{0.75}$ wire-like nanostructures determined with the EDS and EDXRF techniques.

		$Fe_{0.75}Ni_{0.25}$	$Fe_{0.5}Ni_{0.5}$	$Fe_{0.25}Ni_{0.75}$
EDS	Fe [$\%_{mass}$]	63.36	49.82	25.98
	Ni [$\%_{mass}$]	19.02	41.91	66.70
	O [$\%_{mass}$]	17.62	8.27	7.32
Normalized EDS for iron and nickel	Fe [$\%_{mass}$]	76.84	54.28	27.98
	Ni [$\%_{mass}$]	23.16	45.72	72.02
EDXRF	Fe [$\%_{mass}$]	69.63	49.24	26.87
	Ni [$\%_{mass}$]	20.11	40.95	64.27
	other elements [$\%_{mass}$]	10.26	9.81	8.86
Normalized EDXRF for iron and nickel	Fe [$\%_{mass}$]	77.59	54.52	29.48
	Ni [$\%_{mass}$]	22.41	45.48	70.52

across a single chain of $Fe_{0.75}Ni_{0.25}$, $Fe_{0.5}Ni_{0.5}$ and $Fe_{0.25}Ni_{0.75}$ samples are demonstrated in Fig. 2. Considering the line EDS scans across the chains (Fig. 2a, 2c and 2e), they have been collected in order to estimate the oxygen content which is present in the material as well as to eliminate the predominant signal originating from a carbon tape. These two corrections have been very useful in verification of the line EDS scans along chains. Analyzing the obtained results from both EDS profiles, one can see that all investigated chains are mainly composed of iron and nickel. They also contain a small amount of oxygen because the signal associated with oxygen increases slightly when it is collected on the chains. The average oxygen content along all single Fe–Ni chains oscillate around 10%. Studies of the longitudinal EDS profiles indicate that the mass distribution of iron, nickel and oxygen is quite uniform along the entire length of all iron-nickel samples. Finally, the iron, nickel and oxygen contents in the single $Fe_{0.75}Ni_{0.25}$, $Fe_{0.5}Ni_{0.5}$ and $Fe_{0.25}Ni_{0.75}$ nanochains are consistent with the point EDS scans and EDXRF measurements.

As stated before, the presence of oxygen in the EDS spectra is linked with the formation of thin oxide layer on the surface of Fe–Ni nanochains. This assumption is confirmed by the transmission electron microscope (TEM) scans shown in Fig. 3. A dark core region and a light-grey shell layer are clearly distinguishable. The thickness of oxide layer oscillates around 4 nm for all Fe–Ni samples and this is consistent with the previously reported observations describing the initial oxidation of other iron and nickel nanostructures [19,22–34]. Moreover, the TEM data show much better than the SEM images presented in Fig. 1 that all investigated iron-nickel nanostructures are composed of nanoparticles. Analyzing the TEM images, it is also worth noting that the nanoparticles forming the $Fe_{0.75}Ni_{0.25}$ and $Fe_{0.5}Ni_{0.5}$ chains are separated from each other by very thin interface layers, whereas the $Fe_{0.25}Ni_{0.75}$ chains seem to reveal the uniform structure. The electron diffraction (ED) pattern of the $Fe_{0.5}Ni_{0.5}$ sample recorded in a parallel to the TEM measurements is demonstrated in Fig. 3d. In fact, only this pattern is shown here as an example because the other look almost the same. The representative ED spectrum of the Fe–Ni chains consists of two highly diffuse rings. Such pattern is typically obtained for the various materials which reveal nanocrystalline or amorphous nature

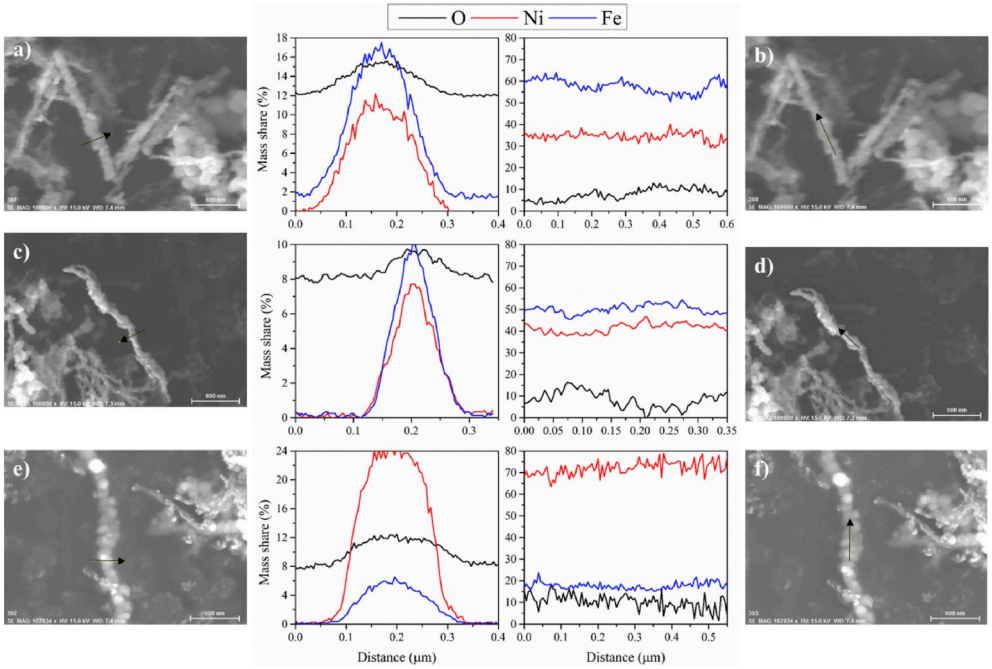

Fig. 2. SEM images and corresponding line EDS profiles **(a)** across and **(b)** along $Fe_{0.75}Ni_{0.25}$, **(c)** across and **(d)** along $Fe_{0.5}Ni_{0.5}$, **(e)** across and **(f)** along $Fe_{0.25}Ni_{0.75}$ wire-like nanostructures; black arrow indicates the direction of the EDS scan.

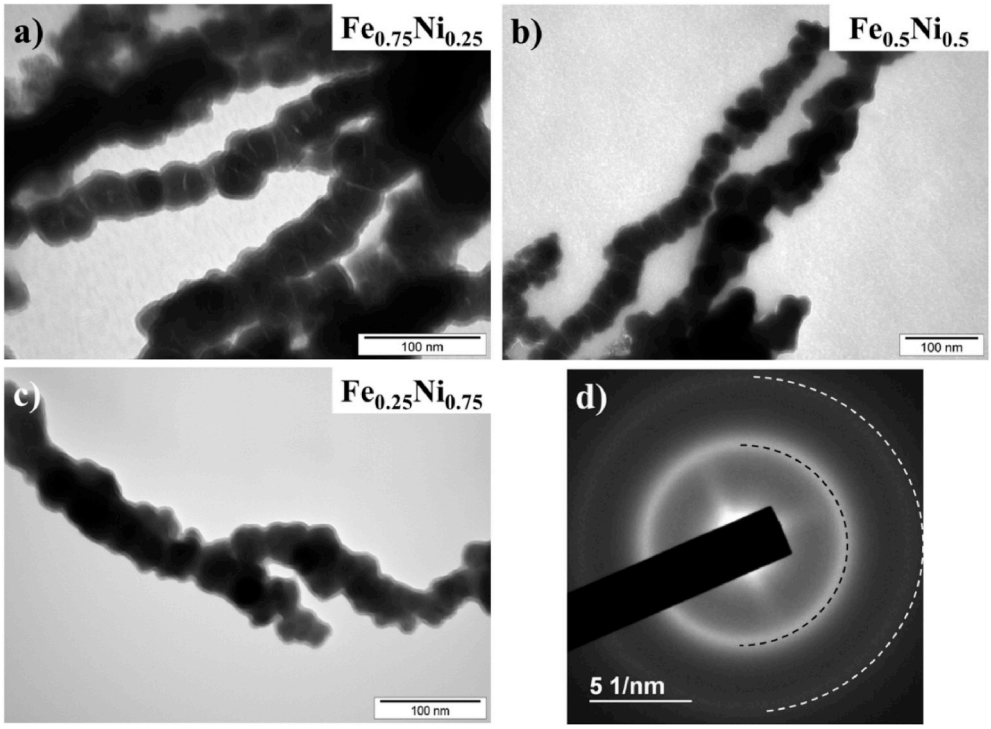

Fig. 3. TEM images of **(a)** $Fe_{0.75}Ni_{0.25}$, **(b)** $Fe_{0.5}Ni_{0.5}$ and **(c)** $Fe_{0.25}Ni_{0.75}$ wire-like nanostructures. **(d)** The electron diffraction pattern recorded for the $Fe_{0.5}Ni_{0.5}$ sample.

[23,28,35–38]. Surprisingly, the positions of recorded ED rings could be faintly fitted to either (111) and (220) or (110) and (211) crystal planes usually observed in the polycrystalline Fe–Ni nanomaterials with a face-centered cubic (fcc) or a body-centered cubic (bcc) structure [18,39–41], respectively, whereas at the same time the (200) plane is vanished for both phases. This indicates that the investigated Fe–Ni chains are amorphous rather than polycrystalline. Moreover, it is worth noting that one of the ED fringes is much more pronounced and broader than the second one. Finally, no signal associated with the presence of oxides is found during the ED measurements. This denotes that the oxide layer is apparently amorphous.

Fig. 4 shows the XRD patterns of the as-prepared iron-nickel wire-like nanomaterials. All patterns were collected using the same experimental conditions i.e. a step of 0.05° and a collecting time of 55 s per each step. This experimental results indicate that the Fe–Ni chains are amorphous because only two very broad peaks are visible in the XRD patterns for all samples. Moreover, it is hardly to assign their positions to the well-defined crystallographic orientations because their maxima are located between the characteristic peak positions of crystalline face-centered cubic (fcc) Fe–Ni (JCPDS card no. 47–1417) and body-centered cubic (bcc) Fe–Ni (JCPDS card no. 37–0474) alloys. Besides the nanometer size of investigated samples, this could be a reason of the significant broadening of the XRD peaks. On the other hand, the XRD patterns of the Fe–Ni nanomaterials consist of only two peaks. One of them is much more intense than the second one. This, in fact, agrees well with the ED measurements. Furthermore, the low crystallinity degree is a common observation for the nanostructures synthesized with the use of sodium borohydride and this is mainly associated with the formation of ultrafine grains and amorphous nature of these materials [19,22,28,34,35,42–44]. Similarly to the previously discussed ED results, no peaks associated with iron, nickel or mixed iron-nickel oxide shells are observed in the XRD patterns for the $Fe_{0.75}Ni_{0.25}$, $Fe_{0.5}Ni_{0.5}$ and $Fe_{0.25}Ni_{0.75}$ samples. This means that these oxide layers are too thin to collect the XRD signal or they are amorphous. In turn, a small peak is visible at 30.5° in the XRD pattern for the $Fe_{0.25}Ni_{0.75}$ chains and it might be ascribed to H_3BO_3 (JCPDS card no. 73–2158).

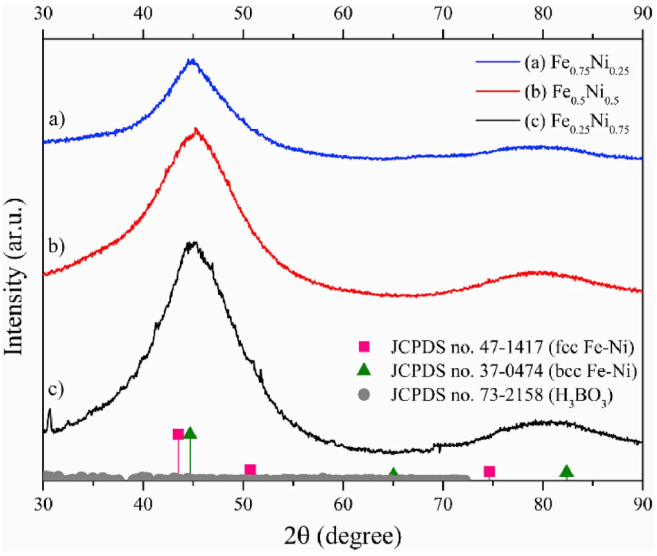

Fig. 4. XRD patterns of **(a)** $Fe_{0.75}Ni_{0.25}$, **(b)** $Fe_{0.5}Ni_{0.5}$ and **(c)** $Fe_{0.25}Ni_{0.75}$ wire-like nanostructures. The peak positions and normalized intensities corresponding to the fcc Fe–Ni, bcc Fe–Ni and H_3BO_3 are assigned according to JCPDS cards and they are marked as squares, triangles and circles, respectively.

The room temperature magnetization hysteresis curves for all Fe–Ni samples are shown in Fig. 5. Their shapes indicate that all wire-like nanostructures behave as the ferromagnetic materials. Further analysis of the hysteresis curves allows identifying two trends. Firstly, the higher concentration of nickel present in the sample the lower their saturation magnetization (M_S at 1 T) values are. The M_S for the $Fe_{0.75}Ni_{0.25}$, $Fe_{0.5}Ni_{0.5}$ and $Fe_{0.25}Ni_{0.75}$ chains equals about 86, 61 and 10 emu/g, respectively. In general, this decrease of M_S value with an increase of Ni content is consistent with the results obtained for the Fe–Ni nanoparticles by M.H. Mokarian et al. [20] who claim that this observation is

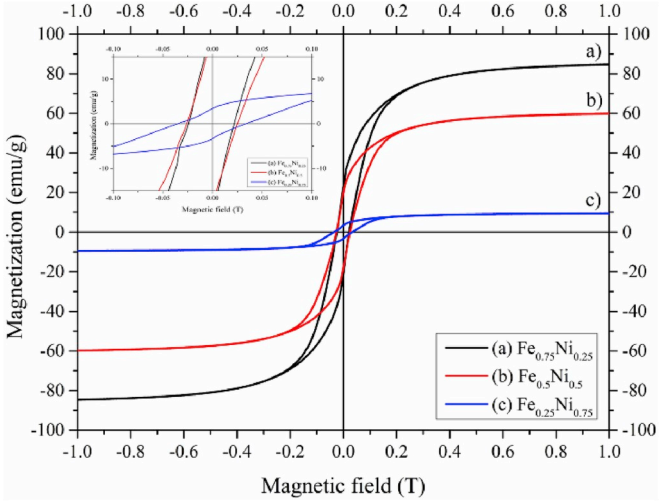

Fig. 5. Room temperature magnetization hysteresis curves of **(a)** $Fe_{0.75}Ni_{0.25}$, **(b)** $Fe_{0.5}Ni_{0.5}$ and **(c)** $Fe_{0.25}Ni_{0.75}$ wire-like nanostructures; inset – magnification of hysteresis in the area of $B = 0$.

associated with the lower magnetic moment of Ni atoms than Fe atoms. It should be also mentioned that the highest reported M_S measured at room temperature for the Fe–Ni nanomaterials can reach even more than 135 emu/g and these values have been obtained for the well crystalline nanomaterials with a nominal composition of $Fe_{0.5}Ni_{0.5}$ [45–47]. Nevertheless, it is worth noting that the M_S of about 62 emu/g has been also measured for the $Fe_{0.5}Ni_{0.5}$ nanoparticles with diameters ranging from 10 to 80 nm by B.Z. Cui et al. [45]. This value is almost the same as for the wire-like nanostructures with similar chemical composition and diameter studied in this work. It is also important that the M_S value obtained for the $Fe_{0.25}Ni_{0.75}$ chains is much lower than for the other investigated samples. In order to explain this issue, it is necessary to recall the electron microscopy experiments which have been discussed before. According the TEM measurements, all Fe–Ni chains reveal the core-shell structures in which the average thickness of the oxide shell is more or less the same. Thus, in the case of $Fe_{0.25}Ni_{0.75}$ nanomaterial, whose average diameter is the lowest among the investigated samples, the impact of oxide shell is the most significant. This leads the weakening of the magnetic response at the applied magnetic fields [19]. Moreover, since the magnetic moment values are given in this work per unit of total mass of whole material (emu/g), the presence of non-magnetic impurities in the $Fe_{0.25}Ni_{0.75}$ chains may also cause the decrease of M_S for this particular sample. Secondly, the increasing amount of nickel present in the sample enhanced their coercivity (H_C). The H_C of the $Fe_{0.75}Ni_{0.25}$, $Fe_{0.5}Ni_{0.5}$ and $Fe_{0.25}Ni_{0.75}$ chains equal 217, 242 and 350 Oe, respectively. The trend mentioned above is rather based on the obtained magnetization hysteresis curves and it is not directly related to the content of nickel in the samples because it depends on many factors such as: size, shape, presence of internal stresses and impurities, ordering and distances between neighboring wire-like chains, etc. At this point, it should be mentioned that the orientation of all studied wire-like chains is random in a respect to the applied field. In a contrary to many other wire-like nanomaterials synthesized using hard or soft templates such as anodized aluminum oxide (AAO) temples or surfactants, the nanochains investigated in this work are not easy to order due to their powder nature. In addition, they can simply interact each other because no barriers against their stacking like template walls or chemical functional groups of surfactants are present. This causes that they form the disordered arrangements which look like the 'partially interweaved stacks of wooden branches' (cf. Fig. 1). Considering all circumstances mentioned above and the difficulties which we have come across during the ordering process of Fe–Ni wire-like nanochains, the magnetic hysteresis measurements have been carried out for the disordered samples. Nevertheless, it is clearly visible that the recorded coercivities for the $Fe_{0.75}Ni_{0.25}$, $Fe_{0.5}Ni_{0.5}$ chains are very similar, whereas the H_C value differs for the $Fe_{0.25}Ni_{0.75}$ sample. Assuming the random orientation of all samples in a respect to the applied field and considering again the real sizes of the investigated Fe–Ni nanostructures traced by the electron microscopy experiments, the average diameter of $Fe_{0.25}Ni_{0.75}$ chains is the lowest, so the ratio between the alloy core and the surface oxide shell is the highest one. In this case, the higher impact of surface oxide layer, which, in fact, might be a magnetically harder material according to the shape of the hysteresis curve shown in the inset of Fig. 5c, is expected. Thus, this may lead to the enhancement of the coercivity for the $Fe_{0.25}Ni_{0.75}$ chains.

Interestingly, the almost similar MFI synthesis have been also performed for the precursor solutions containing Fe^{3+} and Ni^{2+} ions with 1:1 M ratio. In this case, the mixture of nanowires and nanoparticles, which reveal metallic iron structure, has been obtained instead of the bimetallic Fe–Ni wire-like nanostructures (cf. Fig. 6). This can be explained considering two factors: i) values of standard potentials of reduction reactions for ions taken to the reaction, and ii) growth mechanism. In general, the similar iron wire-like nanostructures can be successfully produced in the MFI synthesis using the precursor solutions containing of Fe^{3+} [21,22,34] or Fe^{2+} [37,38] ions. However, the values of standard potentials of reduction reactions for both iron ions are completely different and equal −0.04 V and −0.44 V for Fe^{3+} and Fe^{2+} ions, respectively. This, in fact, causes that the reduction reaction of Fe^{3+} ions occurs faster than the reduction reaction of Fe^{2+} ions [43]. Therefore, in order to perform the co-reduction reactions of iron ions with nickel ions, whose standard potential equals −0.23 V, it is needed to use Fe^{2+} ions. This allows producing nickel nanocrystallites slightly earlier than iron nanocrystallites which then mix and form the bimetallic nanoparticles through coarsening or Ostwald ripening. Afterwards, when the nanoparticles achieve the certain size, they can be aligned along the magnetic field lines due to dipole-dipole interactions [48]. In turn, the MFI synthesis with the precursor solutions containing Fe^{3+} and Ni^{2+} ions leads to the formation of the mixture composed of iron nanowires, iron nanoparticles and nickel material which, in fact, is not bounded with iron nanomaterials. This causes that the nickel is easily removed with other by-products during the cleaning process with the use of the ultrasonic bath.

4. Conclusions

For the first time, this work describes how to manufacture the Fe–Ni wire-like nanostructures with desired iron-to-nickel ratios at room temperature through the simple one-step magnetic-field-induced reduction reaction of precursor solution containing Fe^{2+} and Ni^{2+} ions with aqueous sodium borohydride solution. In a contrary to the previously reported hard or soft temple-assisted methods, the synthesis process descried herein is carried out without use of matrices, surfactants or complexing agents which could introduce the impurities inside the investigated nanomaterials.

The structural and magnetic investigations indicate that the Fe–Ni nanopowders are amorphous core-shell ferromagnetic materials which consist of alloy cores and very thin oxide shells. It is also shown in this work that the increasing content of nickel in the as-prepared Fe–Ni nanostructures influences directly their sizes and indirectly their magnetic parameters like saturation magnetization and coercivity. Moreover, the as-prepared nanomaterials are stable at ambient conditions. Therefore, they can be of interest for application in catalysis, electromagnetic shielding, microwave-absorbents as well as magnetic field sensors [14–17].

Declaration of competing interest

The authors declare that they have no known competing financial interests or personal relationships that could have appeared to influence

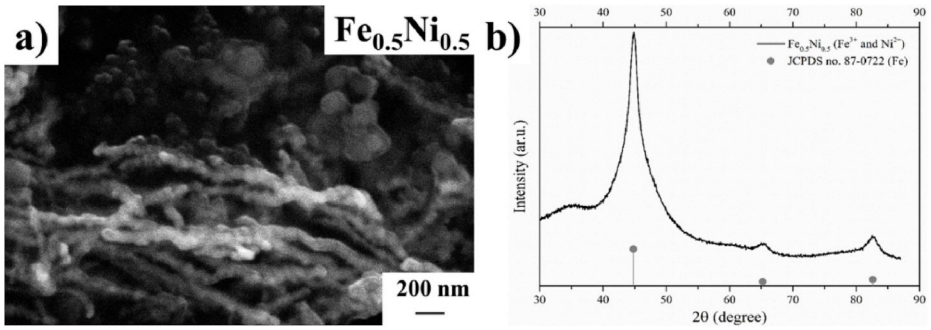

Fig. 6. **(a)** SEM image and **(b)** XRD pattern of as-prepared nanomaterials obtained in the MFI synthesis in which the precursor solution contained Fe^{3+} ions instead of Fe^{2+} ions. The peak positions and normalized intensities corresponding to the Fe are assigned according to JCPDS card and they are marked as circles.

the work reported in this paper.

CRediT authorship contribution statement

Marcin Krajewski: Conceptualization, Formal analysis, Funding acquisition, Investigation, Methodology, Project administration, Resources, Supervision, Visualization, Writing - original draft, Writing - review & editing. **Mateusz Tokarczyk:** Data curation, Investigation. **Tomasz Stefaniuk:** Data curation, Investigation. **Hanna Słomińska:** Investigation. **Artur Małolepszy:** Investigation. **Grzegorz Kowalski:** Investigation, Supervision. **Sabina Lewińska:** Data curation, Investigation, Formal analysis, Writing - review & editing. **Anna Ślawska-Waniewska:** Investigation, Supervision.

Acknowledgements

This work was supported by the National Science Centre (Poland) under grant no. 2016/23/D/ST8/03268. Authors would like to thank Mr. Ryszard Strzałkowski from the Institute of Fundamental Technological Research Polish Academy of Sciences and Dr. Wen-An Chiou from the Advanced Imaging and Microscopy Laboratory belong to the University of Maryland for their support in the performance of transmission electron microscopy and electron diffraction investigations.

Appendix A. Supplementary data

Supplementary data to this article can be found online at https://doi.org/10.1016/j.matchemphys.2020.122812.

References

[1] J. Wang, L.Y. Zhang, P. Liu, T.M. Lan, J. Zhang, L.M. Wei, E.S.W. Kong, C.H. Jiang, Y.F. Zhang, Preparation and growth mechanism of nickel nanowires under applied magnetic field, Nano-Micro Lett. 2 (2010) 134–138, https://doi.org/10.5101/nml.v2i2.p134-138.

[2] N.P. Dasgupta, J.W. Sun, C. Liu, S. Brittman, S.C. Andrews, J. Lim, H.W. Gao, R. X. Yan, P.D. Yang, 25th anniversary article: semiconductor nanowires – synthesis, characterization, and applications, Adv. Mater. 26 (2014) 2137–2184, https://doi.org/10.1002/adma.201305929.

[3] G.S. Ma, X.G. Wang, Synthesis and applications of one-dimensional porous nanowire arrays: a review, Nano 10 (2015) 1530001, https://doi.org/10.1142/S1793292015300017.

[4] M. Krajewski, Magnetic-field-induced synthesis of magnetic wire-like micro- and nanostructures, Nanoscale 9 (2017) 16511–16545, https://doi.org/10.1039/c7nr05823c.

[5] K.Q. Peng, X. Wang, L. Li, Y. Hu, S.T. Lee, Silicon nanowires for advanced energy conversion and storage, Nano Today 8 (2013) 75–97, https://doi.org/10.1016/j.nantod.2012.12.009.

[6] Y.Q. Zhang, B. Ouyang, J. Xu, G.C. Jia, S. Chen, R.S. Rawat, H.J. Fan, Rapid synthesis of cobalt nitride nanowires: highly efficient and low-cost catalysts for oxygen evolution, Angew. Chem. Int. Ed. 55 (2016) 8670–8674, https://doi.org/10.1002/anie.201604372.

[7] J.F. Fennell, S.F. Liu, J.M. Azzarelli, J.G. Weis, S. Rochat, K.A. Mirica, J. B. Ravnsbaek, T.M. Swager, Nanowire chemical/biological sensors: status and a roadmap for the future, Angew. Chem. Int. Ed. 55 (2016) 1266–1281, https://doi.org/10.1002/anie.201505308.

[8] G.H. Lee, S.H. Huh, J.W. Jeong, S.H. Kim, B.J. Choi, H.C. Ri, B. Kim, J.H. Park, Arrays of ferromagnetic FeCo and FeCr binary nanocluster wires, J. Appl. Phys. 94 (2003) 4179, https://doi.org/10.1063/1.1602955.

[9] M.J. Hu, B. Lin, S.H. Yu, Magnetic field-induced solvothermal synthesis of one-dimensional assemblies of Ni–Co alloy microstructures, Nano Res 1 (2008) 303–313, https://doi.org/10.1007/s12274-008-8031-6.

[10] M.Z. Wu, G.Q. Liu, M.T. Li, P. Dai, Y.Q. Ma, L.D. Zhang, Magnetic field-assisted solvothermal assembly of one-dimensional nanostructures of Ni–Co alloy nanoparticles, J. Alloys Compd. 491 (2010) 689–693, https://doi.org/10.1016/j.jallcom.2009.10.273.

[11] Q. Sun, S.G. Wang, R.M. Wang, Well-aligned CoPt hollow nanochains synthesized in water at room temperature, J. Phys. Chem. C 116 (2012) 5352–5357, https://doi.org/10.1021/jp210144p.

[12] H. Wang, X.Y. Li, M. Li, K.N. Xie, L. Liao, Preparation of Ni/Cu composite nanowires, Beilstein J. Nanotechnol. 6 (2015) 1268–1271, https://doi.org/10.3762/bjnano.6.130.

[13] M. Krajewski, M. Tokarczyk, T. Stefaniuk, S. Lewińska, A. Ślawska-Waniewska, Thermal treatment of chains of amorphous $Fe_{1-x}Co_x$ nanoparticles made by magnetic-field-induced coreduction reaction, IEEE Magn. Lett. 10 (2019) 6108405, https://doi.org/10.1109/lmag.2019.2950644.

[14] Y.J. Zou, J. Cheng, Q.Y. Wang, C.L. Xiang, H.L. Chu, S.J. Qiu, H.Z. Zhang, F. Xu, S. S. Liu, C.Y. Tang, L.X. Sun, Cobalt-boron/nickel-boron nanocomposite with improved catalytic performance for the hydrolysis of ammonia borane, Int. J. Hydrogen Energy 40 (2015) 13423–13430, https://doi.org/10.1016/j.ijhydene.2015.08.017.

[15] H.H. Wu, M. Zeng, Z.Y. Li, X. Zhu, C.C. Tian, C.G. Xia, L. He, S. Dai, Coupling FeNi alloys and hollow nitrogen-enriched carbon frameworks leads to high-performance oxygen electrocatalysts for rechargeable zinc–air batteries, Sustain. Energ. Fuels 3 (2019) 136–141, https://doi.org/10.1039/c8se00362a.

[16] J. Zhou, Z.H. Zhu, C. Xiong, Synthesis, electromagnetic and wave-absorbing properties of a FeNi alloy nano-whisker/particle mixture, J. Electron. Mater. 47 (2018) 1244–1249, https://doi.org/10.1007/s11664-017-5856-3.

[17] T.I. Zubar, S.A. Sharko, D.I. Tishkevich, N.N. Kovaleva, D.A. Vinnik, S.A. Gudkova, E.L. Trukhanova, E.A. Trofimov, S.A. Chizhik, L.V. Panina, S.V. Trukhanov, A. V. Trukhanov, Anomalies in Ni-Fe nanogranular films growth, J. Alloys Compd. 748 (2018) 970–978, https://doi.org/10.1016/j.jallcom.2018.03.245.

[18] Q.F. Liu, J.B. Wang, Z.J. Yan, D.S. Xue, Characterization and magnetic properties of $Fe_{1-x}Ni_x$ nanowire arrays, Phys. Rev. B 72 (2005) 144412, https://doi.org/10.1103/PhysRevB.72.144412.

[19] A.P. Douvalis, R. Zboril, A.B. Bourlinos, J. Tucek, S. Spyridi, T. Bakas, A facile synthetic route toward air-stable magnetic nanoalloys with Fe–Ni/Fe–Co core and iron oxide shell, J. Nanopart. Res. 14 (2012) 1130, https://doi.org/10.1007/s11051-012-1130-z.

[20] M.H. Mokarian, M. Almasi-kashi, S. Alikhanzadeh-Arani, A. Ramazani, The fcc/bcc phase transition in Fe_xNi_{100-x} nanoparticles resolved by first-order reversal curves, J. Mater. Sci. 52 (2017) 7831–7842, https://doi.org/10.1007/s10853-017-1025-6.

[21] W.S. Lin, Z.J. Jian, H.M. Lin, L.C. Lai, W.A. Chiou, Y.K. Hwu, S.H. Wu, W.C. Chen, Y.D. Yao, Synthesis and characterization of iron nanowires, J. Chin. Chem. Soc. 60 (2013) 85–91, https://doi.org/10.1002/jccs.201200263.

[22] M. Krajewski, W.S. Lin, H.M. Lin, K. Brzozka, S. Lewinska, N. Nedelko, A. Slawska-Waniewska, J. Borysiuk, D. Wasik, Structural and magnetic properties of iron nanowires and iron nanoparticles fabricated through a reduction reaction, Beilstein J. Nanotechnol. 6 (2015) 1652–1660, https://doi.org/10.3762/bjnano.6.167.

[23] A. Roy, V. Srinivas, S. Ram, J.A. De Toro, U. Mizutani, Structure and magnetic properties of oxygen-stabilized tetragonal Ni nanoparticles prepared by borohydride reduction method, Phys. Rev. B 71 (2005) 184443, https://doi.org/10.1103/PhysRevB.71.184443.

[24] L.T. Kuhn, A. Bojesen, L. Timmermann, M.M. Nielsen, S. Morup, Structural and magnetic properties of core–shell iron–iron oxide nanoparticles, J. Phys.-Condes. Matter 14 (2002) 13551–13567, https://doi.org/10.1088/0953-8984/14/49/311.

[25] L. Signorini, L. Pasquini, L. Savini, R. Carboni, F. Boscherini, E. Bonetti, A. Giglia, M. Pedio, N. Mahne, S. Nannarone, Size-dependent oxidation in iron/iron oxide core-shell nanoparticles, Phys. Rev. B 68 (2003) 195423, https://doi.org/10.1103/PhysRevB.68.195423.

[26] E.E. Carpenter, S. Calvin, R.M. Stroud, V.G. Harris, Passivated iron as core-shell nanoparticles, Chem. Mater. 15 (2003) 3245–3246, https://doi.org/10.1021/cm034131l.
[27] C.M. Wang, D.R. Baer, L.E. Thomas, J.E. Amonette, J. Antony, Y. Qiang, G. Duscher, Void formation during early stages of passivation: initial oxidation of iron nanoparticles at room temperature, J. Appl. Phys. 98 (2005), 094308, https://doi.org/10.1063/1.2130890.
[28] J.T. Nurmi, P.G. Tratnyek, V. Sarathy, D.R. Baer, J.E. Amonette, K. Pecher, C. M. Wang, J.C. Linehan, D.E. Matson, R.L. Penn, M.D. Driessen, Characterization and properties of metallic iron nanoparticles: spectroscopy, electrochemistry, and kinetics, Environ. Sci. Technol. 39 (2005) 1221–1230, https://doi.org/10.1021/es049190u.
[29] Y. Qiang, J. Antony, A. Sharma, J. Nutting, D. Sikes, D. Meyer, Iron/iron oxide core-shell nanoclusters for biomedical applications, J. Nanopart. Res. 8 (2006) 489–496, https://doi.org/10.1007/s11051-005-9011-3.
[30] C.M. Wang, D.R. Baer, J.E. Amonette, M.H. Engelhard, J. Antony, Y. Qiang, Morphology and electronic structure of the oxide shell on the surface of iron nanoparticles, J. Am. Chem. Soc. 131 (2009) 8824–8832, https://doi.org/10.1021/ja900353f.
[31] A.C. Johnston-Peck, J.W. Wang, J.B. Tracy, Synthesis and structural and magnetic characterization of Ni(Core)/NiO(Shell) nanoparticles, ACS Nano 3 (2009) 1077–1084, https://doi.org/10.1021/nn900019x.
[32] J.G. Railsback, A.C. Johnston-Peck, J.W. Wang, J.B. Tracy, Size-dependent nanoscale Kirkendall effect during the oxidation of nickel nanoparticles, ACS Nano 4 (2010) 1913–1920, https://doi.org/10.1021/nn901736y.
[33] S.Y. Wei, Q. Wang, J.H. Zhu, L.Y. Sun, H.F. Lin, Z.H. Guo, Multifunctional composite core-shell nanoparticles, Nanoscale 3 (2011) 4474–4502, https://doi.org/10.1039/c1nr11000d.
[34] M. Krajewski, K. Brzozka, W.S. Lin, H.M. Lin, M. Tokarczyk, J. Borysiuk, G. Kowalskia, D. Wasik, High temperature oxidation of iron-iron oxide core-shell nanowires composed of iron nanoparticles, Phys. Chem. Chem. Phys. 18 (2016) 3900–3909, https://doi.org/10.1039/c5cp07569f.
[35] B. Yang, Y. Wu, X.P. Li, R.H. Yu, Chemical synthesis of high-stable amorphous FeCo nanoalloys with good magnetic properties, Nanomaterials 8 (2018) 154, https://doi.org/10.3390/nano8030154.
[36] K.V.P.M. Shafi, A. Gedanken, R. Prozorov, Sonochemical preparation and characterization of nanosized amorphous Co–Ni alloy powders, J. Mater. Chem. 8 (1998) 769–773, https://doi.org/10.1039/a706871i.
[37] S.A. Mansour, Non-isothermal crystallization kinetics of nano-sized amorphous TiO_2 prepared by facile sonochemical hydrolysis route, Ceram. Int. 45 (2019) 2893–2898, https://doi.org/10.1016/j.ceramint.2018.07.273.
[38] R. Babilas, A. Bajorek, L. Temleitner, Structural study of amorphous and nanocrystalline Mg-based metallic glass examined by neutron diffraction, X-ray photoelectron spectroscopy, Reverse Monte Carlo calculations and high-resolution electron microscopy, J. Non-Cryst. Solids 505 (2019) 421–430, https://doi.org/10.1016/j.jnoncrysol.2018.11.025.
[39] G. Chieffi, C. Giordano, M. Antonietti, D. Esposito, FeNi nanoparticles with carbon armor as sustainable hydrogenation catalysts: towards biorefineries, J. Mater. Chem. 2 (2014) 11591–11596, https://doi.org/10.1039/c4ta02457e.
[40] H.Z. Yang, Y. Li, M. Zeng, W. Cao, W.E. Bailey, R.H. Yu, Static and dynamic magnetization of gradient FeNi alloy nanowire, Sci. Rep. 6 (2016) 20427, https://doi.org/10.1038/srep20427.
[41] Y. Hong, Y. Rheem, M. Lai, D.M. Cwiertny, S.L. Walker, N.V. Myung, Electrochemical synthesis of Fe_xNi_{1-x} nanostructures for environmental remediation, Chem. Eng. J. 151 (2009) 66–72, https://doi.org/10.1016/j.cej.2009.01.048.
[42] X.Y. Yang, B. Yang, X.P. Li, Y. Cao, R.H. Yu, Structural-controlled chemical synthesis of nanosized amorphous Fe particles and their improved performances, J. Alloys Compd. 651 (2015) 551–556, https://doi.org/10.1016/j.jallcom.2015.08.156.
[43] G.N. Glavee, K.J. Klabunde, C.M. Sorensen, G.C. Hadjipanayis, Chemistry of borohydride reduction of iron(II) and iron(III) ions in aqueous and nonaqueous media. Formation of nanoscale Fe, FeB, and Fe_2B powders, Inorg. Chem. 34 (1995) 28–35, https://doi.org/10.1021/ic00105a009.
[44] N.B. Nayak, B.B. Nayak, A. Mondal, Enhanced activation energy of crystallization of pure zirconia nanopowders prepared via an efficient way of synthesis using $NaBH_4$, J. Am. Ceram. Soc. 96 (2013) 3366–3368, https://doi.org/10.1111/jace.12605.
[45] B.Z. Cui, M. Marinescu, J.F. Liu, High magnetization Fe-Co and Fe-Ni submicron and nanosize particles by thermal decomposition and hydrogen reduction, J. Appl. Phys. 115 (2014) 17A315, https://doi.org/10.1063/1.4863806.
[46] X.Y. Zhang, Y. Liu, J. Li, X.J. Yang, Synthesis and magnetic studies of Fe–Ni nanofibres by electrospinning, Mater. Res. Innovat. 17 (2013) 436–439, https://doi.org/10.1179/1433075X11Y.0000000065.
[47] N.S. Kanhe, A. Kumar, S.M. Yusuf, A.B. Nawale, S.S. Gaikwad, S.A. Raut, S. V. Bhoraskar, S.Y. Wu, A.K. Das, V.L. Mathe, Investigation of structural and magnetic properties of thermal plasma-synthesized $Fe_{1-x}Ni_x$ alloy nanoparticles, J. Alloys Compd. 663 (2016) 30–40, https://doi.org/10.1016/j.jallcom.2015.11.190.
[48] X.Y. Li, H. Wang, K.N. Xie, Q. Long, X.F. Lai, L. Liao, Self-assembly mechanism of Ni nanowires prepared with an external magnetic field, Beilstein J. Nanotechnol. 6 (2015) 2123–2128, https://doi.org/10.3762/bjnano.6.217.